ACTA ASTRONAUTICA

(SPONSORED BY THE INTERNATIONAL ACADEMY OF ASTRONAUTICS)

MANUSCRIPT ID: AA_2015_228: Impact Factor: 1.095; ISSN: 0094-5765

ACCEPTED JUNE 23RD 2016

MHD DISSIPATIVE FLOW AND HEAT TRANSFER OF CASSON FLUIDS DUE TO METACHRONAL WAVE PROPULSION OF BEATING CILIA WITH THERMAL AND VELOCITY SLIP EFFECTS UNDER AN OBLIQUE MAGNETIC FIELD

Noreen Sher Akbar[1], D. Tripathi[2]*, O. Anwar Bég[3] and Z.H. Khan[4]

[1]*DBS&H, CEME, National University of Sciences and Technology, Islamabad, Pakistan*
[2]*Department of Mechanical Engineering, Manipal University, Jaipur-303007, India*
[3]*Fluid Mechanics, Spray Research Group, Petroleum and Gas Engineering Division, University of Salford, Newton Building, G77, The Crescent, Salford, M54WT, England, UK.*
[4]*Department of Mathematics, University of Malakand, Chakdara, Dir (Lower), Khyber Pakhtunkhwa, Pakistan.*

ABSTRACT

A theoretical investigation of magnetohydrodynamic (MHD) flow and heat transfer of electrically-conducting viscoplastic fluids through a channel is conducted. The robust Casson model is implemented to simulate viscoplastic behavior of fluids. The external magnetic field is oblique to the fluid flow direction. Viscous dissipation effects are included. The flow is controlled by the metachronal wave propagation generated by cilia beating on the inner walls of the channel. The mathematical formulation is based on deformation in longitudinal and transverse velocity components induced by the ciliary beating phenomenon with cilia assumed to follow elliptic trajectories. The model also features velocity and thermal slip boundary conditions. Closed-form solutions to the non-dimensional boundary value problem are obtained under physiological limitations of low Reynolds number and large wavelength. The influence of key hydrodynamic and thermo-physical parameters i.e. Hartmann (magnetic) number, Casson (viscoplastic) fluid parameter, thermal slip parameter and velocity slip parameter on flow characteristics are investigated. A comparative study is also made with Newtonian fluids (corresponding to massive values of plastic viscosity). Stream lines are plotted to visualize trapping phenomenon. The computations reveal that velocity increases with increasing the magnitude of Hartmann number near the channel walls whereas in the core flow region (centre of the channel) significant deceleration is observed. Temperature is elevated with greater Casson parameter, Hartmann number, velocity slip, eccentricity parameter, thermal slip and also Brinkmann (dissipation) number. Furthermore greater Casson parameter is found to elevate the quantity and size of the trapped bolus. In the pumping region, the pressure rise is reduced with greater Hartmann number, velocity slip, and wave number whereas it is enhanced with greater cilia length.

Keywords: *Heat Transfer; Brinkmann number; Cilia motion; Viscoplastic fluids; Oblique Magnetic field; Slip Boundary Conditions; Metachronal wave propagation.*

*Corresponding Author: dharmtri@gmail.com (D Tripathi)

NOMENCLATURE:

x, y coordinates	***Greek Symbols***
p pressure	ε cilia length
u, v velocity components	λ wavelength
S_{ij} stress tensor	γ thermal slip parameter
Re Reynolds number	Λ velocity slip parameter
M Hartmann number	α measure of eccentricity
Ec Eckert number,	ζ Casson parameter
Br Brinkman number	μ_B plastic viscosity of the fluid
Pr Prandtl number	Θ inclination of magnetic field
c wave number	σ electrical conductivity of Casson fluid
a half width of the channel	ρ density of Casson fluid
c_p specific heat at constant pressure	k thermal conductivity of Casson fluid
p_y yield stress of Casson fluid	β wave number

1. INTRODUCTION

Driven by the realization that numerous proteins involved in mammalian diseases localize to basal bodies and cilia, and that the aberrant ciliary function can be linked to a large number of human diseases and syndromes, extraordinary progress has been achieved over the past few decades. Cilia are present on the majority of mammalian cells throughout development and feature prominently in the adult life of an organism. They are found to be associated with a variety, often overlapping, of clinical abnormalities affecting the function of numerous tissues and organs including epithelium of the respiratory tract, oviduct, testes, brain, kidney, eye, inner ear, and olfactory epithelium. Defects in the respiratory tract manifest as rhinitis, sinusitis, otitis media or bronchiectasis [1]. Ciliary movement occurs in the axoneme by the unidirectional sliding of the outer doublets of microtubules generated by the adenosine triphosphate (ATP)-energized dynein arms. It can be assessable in the absence of membrane or ciliary matrix and can

be reproduced on "models" of cilia whose membrane has been partially or completely destroyed by detergents. Thus, isolated cilia or flagella, or "models" of whole ciliates (for instance, Paramecium), gently treated with Triton X-100, can be re-activated and are able to swim normally when they are bathed in an appropriate medium whose main components are the specific substrates for dynein. The complex dynamics of cilia has therefore stimulated substantial attention in mathematical biology and bioengineering. Sleigh [2] studied the biology of cilia and flagella and discussed the propulsion of cilia as a metachronic wave and emphasized their significance in propulsion. Miller [3] investigated the movement of Newtonian fluids initiated and sustained by mechanical cilia. Blake [4] extended Sleigh's work from a mathematical perspective and employed a spherical envelope approach to analyze ciliary propulsion. Blake [5] further presented comprehensive mathematical results for cilia-induced Stokes flows in tubules, considering the array coordination as a metachronal wave. Khaderi *et al*. [6] investigated rigorously the mechanics and performance of magnetically-driven artificial cilia for lab-on-a-chip applications. Dauptain *et al.* [7] addressed both analytically and numerically the hydrodynamics of ciliary propulsion. Khaderi *et al.* [8] again reported interesting results concerning their observations that the metachronal motion of symmetrically beating cilia establishes a *net pressure gradient in the direction of the metachronal wave*, which creates a uni-directional flow field. In another article, Khaderi and Onck [9] further developed a numerical model to simulate in some detail, the interaction of magnetic artificial cilia with surrounding fluids in three-dimensional viscous flow. In this direction, some substantial extensions [10-12] have been made to refine mathematical models of cilia hydrodynamics.

Many physiological fluids can be characterized as *viscoplastic fluids* which are a sub-branch of rheological liquids possessing both *viscous* and *plastic* properties. Plasticity is characterized by a yield stress, below which the materials will not deform, and above which they will deform and flow according to different constitutive relations. Some popular viscoplastic models which have emerged, largely from chemical engineering research, are the Bingham plastic [13], the Herschel Bulkley model [14], and the Casson model [15], [16]. Bird *et al.* [17] elaborated extensively on the diverse rheology of viscoplastic materials and their associated hydrodynamic characteristics. Numerous researchers have utilized viscoplastic models [18-22] to more accurately mimic realistically the dynamics of blood flow and also food bolus movement in digestive system. The

Casson model has proved to be quite advantageous in this regard as it is relatively simple but provides comparatively accurate representation of the shear-stress strain characteristics of actual biological liquids.

The inner surfaces of physiological vessels are generally smooth and hydrophobic in nature. This leads to the possibilities of hydrodynamic and thermal slipping of fluids during physiological transport. Since many biological processes involve both flow and heat transfer (e.g. blood is heat-conducting), researchers have explored both hydrodynamic (velocity) and thermal slip effects. Cottin-Bizonne *et al*. [23] have studied the boundary slip on smooth hydrophobic surface. They employed a dynamic surface force apparatus to evaluate more precisely the hydrodynamic boundary condition of simple liquids flowing on smooth hydrophobic surfaces and suggested possible mechanisms for large slip length on smooth hydrophobic surfaces caused by hydrophobic particle contamination. Ngoma and Erchiqui [24] investigated thermal and slip effects on fluid flow through microchannels, observing that for pressure-driven electro-osmotic flows, slip coefficient exerts a significant effect on flow velocity, local temperature and Nusselt number. In the context of hemodynamics, Misra and Schit [25] addressed the role of slip velocity in blood flow through arteries using the Herschel–Bulkley equation, and examining mild, moderate, and severe stenosis growth at the lumen. They found that slip influences significantly the volumetric flow rate of blood, flow resistance and also wall (skin) friction. Ebaid [26] discussed the effects of magnetic field and wall slip conditions on peristaltic transport. Yilmaz and Gundogdu [27] reviewed the blood flow in large arteries and analyzed the role of slipping. Ellahi [28] studied with the homotopy analysis method the Oldroyd 8-constant non-Newtonian slip flow in a channel. Srinivas *et al.* [29] investigated the effects of heat transfer, magnetic fields and slip condition on peristaltic transport, observing that with great Knudsen number (slip effect), the quantity of trapped boluses is markedly increased. Uddin *et al.* [30] considered thermal, velocity and mass slip effects on bioconvection nanofluid flow with wall transpiration, showing that increased thermal slip decelerates the flow, whereas greater mass (solutal) slip accelerates the flow and also elevates temperatures but suppresses nano-particle concentration. Tripathi [31] examined slip effects on peristaltic flow of couple stress fluids through a porous channel. Akbar and Nadeem [32] computed thermal and velocity slip effects on peristaltic transport of viscoelastic fluids with the Jeffrey model. Latiff *et al.* [33] studies thermal and

velocity slip on transient micropolar slip flow from a stretching/shrinking sheet with the numerical quadrature MAPLE code. Tripathi *et al*. [34] used the homotopy method to analyze slip effects on peristaltic viscoelastic propulsion. All these studies confirmed the non-trivial influence of slip effects on biofluid dynamics processes.

In light of the above works, it is evident that numerous simulations have been conducting relating to cilia induced flow, MHD flow, flow of Casson fluids through various type of geometries and peristaltic transport in the presence or absence of thermal and velocity slip conditions. However, thusfar, to the authors' knowledge, the problem of *viscoplastic flow due to metachronal wave propulsion generated by cilia beationg under the effects of inclined magnetic field and thermal and velocity slip effects*, has yet to be addressed. In the present article, we therefore consider two-dimensional flow of Casson fluid through an oscillating channel with the distensible walls lined with homogenous cilia structures. An inclined (oblique) magnetic field is applied to control the flow. Thermal and velocity boundary conditions are taken into account. Lubrication theory is employed to simplify the coupling governing non-linear equations. The influence of magnetic field, Casson fluid parameter, cilia geometry, thermal and velocity slip parameters and also viscous heating parameter (Brinkmann number) on cilia movement and thermo-fluid dynamic characteristics (pressure, velocity, temperature) is evaluated and furthermore discussed with the help of illustrations. The present investigation is relevant to the analysis of magnetically-controlled surface-modified biomimetic pumps in medical engineering [35] and is in particular aimed at evaluating in more detail rheological working fluid, geometric and heat transfer effects on the flow characteristics.

2. MATHEMATICAL FORMULATION

Let us consider the heat transfer and flow of an incompressible electrically-conducting Casson non-Newtonian fluid through a symmetric channel with thermal and velocity slip boundary conditions imposed at the channel walls. Viscous dissipation is incorporated. We choose Cartesian coordinates (Y, X), where X -axis lies along the centre of the channel and Y is transverse to it. The channel flow is regulated by an oblique static magnetic field imposed at an angle Θ to the X-axis. This generates both horizontal and vertical components of Lorentzian

magnetohydrodynamic body force, which have been elaborated earlier in detail by Bég *et al.* [36] and Ghosh *et al*. [37]. When the angle Θ becomes 90 degrees, the field is imposed *transverse* to the *X*-direction (i.e. aligned with the *Y*-direction). Flow is generated due to a metachronal wave which is produced by the collective, rhythmic beating of the cilia with constant wave speed, *c*, along the channel walls which have inner surfaces that are ciliated. A constant temperature, T_0, is prescribed at the channel walls. The geometry of the wall surface is shown in **Fig.1.** and expressed as :

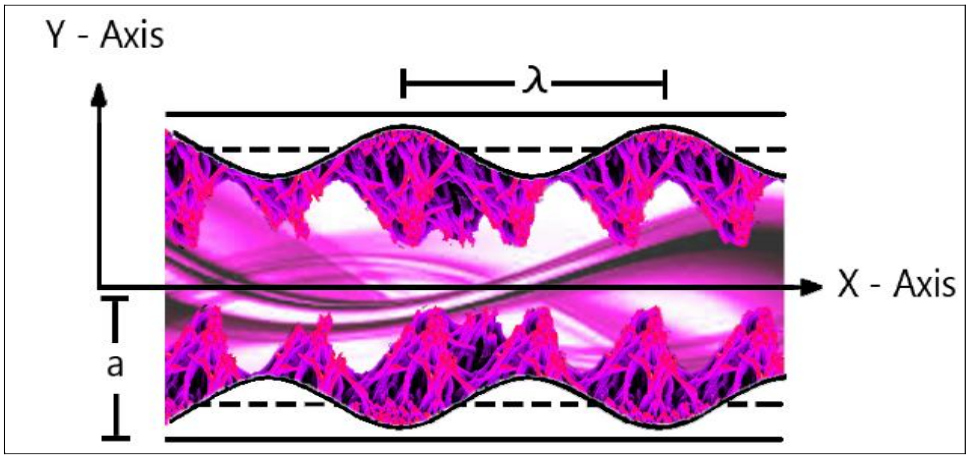

Fig.1. Geometry of the problem.

$$\bar{Y} = \pm\left[a + a\varepsilon \cos\left(\frac{2\pi}{\lambda}(\bar{X} - c\bar{t}) \right) \right] = \pm H \,. \tag{1}$$

Sleigh [2] observed that cilia tips move in *elliptical paths*. In line with this approach, the vertical position of the cilia tips can be written as:

$$\bar{X} = X_0 + a\varepsilon\alpha \sin\left(\frac{2\pi}{\lambda}(\bar{X} - c\bar{t}) \right). \tag{2}$$

The horizontal and vertical velocities of the cilia are given as:

$$U_0 = \frac{-\left(\frac{2\pi}{\lambda}\right) a\varepsilon\alpha c_1 \cos\left(\frac{2\pi}{\lambda}\left(\bar{X} - c\bar{t}\right)\right)}{1 - \left(\frac{2\pi}{\lambda}\right) a\varepsilon\alpha c_1 \cos\left(\frac{2\pi}{\lambda}\left(\bar{X} - c\bar{t}\right)\right)}, \tag{3}$$

$$V_0 = \frac{-\left(\frac{2\pi}{\lambda}\right) a\varepsilon\alpha c_1 \sin\left(\frac{2\pi}{\lambda}\left(\bar{X} - c\bar{t}\right)\right)}{1 - \left(\frac{2\pi}{\lambda}\right) a\varepsilon\alpha c_1 \sin\left(\frac{2\pi}{\lambda}\left(\bar{X} - c\bar{t}\right)\right)}. \tag{4}$$

The governing equations (mass, momentum and energy conservation equations) for two-

dimensional unsteady flow of incompressible viscoplastic fluids under the effects of inclined magnetic field and heat transfer may be presented as follows:

$$\frac{\partial \bar{U}}{\partial \bar{X}}+\frac{\partial \bar{V}}{\partial \bar{Y}}=0, \tag{5}$$

$$\rho\left(\frac{\partial}{\partial \bar{t}}+\bar{U}\frac{\partial}{\partial \bar{X}}+\bar{V}\frac{\partial}{\partial \bar{Y}}\right)\bar{U}=-\frac{d\bar{P}}{d\bar{X}}+\frac{\partial}{\partial \bar{X}}\left(\bar{S}_{\bar{X}\bar{X}}\right)+\frac{\partial}{\partial \bar{Y}}\left(\bar{S}_{\bar{X}\bar{Y}}\right)+\sigma {B_o}^2\bar{U}\cos\Theta, \tag{6}$$

$$\rho\left(\frac{\partial}{\partial \bar{t}}+\bar{U}\frac{\partial}{\partial \bar{X}}+\bar{V}\frac{\partial}{\partial \bar{Y}}\right)\bar{V}=-\frac{d\bar{P}}{d\bar{Y}}+\frac{\partial}{\partial \bar{X}}\left(\bar{S}_{\bar{Y}\bar{X}}\right)+\frac{\partial}{\partial \bar{Y}}\left(\bar{S}_{\bar{Y}\bar{Y}}\right)+\sigma {B_o}^2\bar{V}\sin\Theta, \tag{7}$$

$$\rho c_p\left(\frac{\partial \bar{T}}{\partial \bar{t}}+\bar{U}\frac{\partial \bar{T}}{\partial \bar{X}}+\bar{V}\frac{\partial \bar{T}}{\partial \bar{Y}}\right)=\frac{\partial \bar{U}}{\partial \bar{X}}\left(\bar{S}_{\bar{X}\bar{X}}\right)+\frac{\partial \bar{V}}{\partial \bar{X}}\left(\bar{S}_{\bar{X}\bar{Y}}\right)+\frac{\partial \bar{U}}{\partial \bar{Y}}\left(\bar{S}_{\bar{Y}\bar{X}}\right)+\frac{\partial \bar{V}}{\partial \bar{Y}}\left(\bar{S}_{\bar{Y}\bar{Y}}\right)+k\left(\frac{\partial^2 \bar{T}}{\partial \bar{X}^2}+\frac{\partial^2 \bar{T}}{\partial \bar{Y}^2}\right), \tag{8}$$

The last terms in eqn. (6) and (7) denote the magnetohydrodynamic body force components. The stress tensor for an isotropic flow of a Casson fluid can be expressed as (Eldabe and Silwa [38]):

$$S_{ij}=\begin{cases}2e_{ij}\left(\mu_B+s_y/\sqrt{2\pi}\right), \pi \succ \pi_c,\\ 2e_{ij}\left(\mu_B+s_y/\sqrt{2\pi}\right), \pi \prec \pi_c\end{cases} \tag{9}$$

where s_y is the yield stress of the fluid, $\pi=e_{ij}e_{ij}$, (product of the component of deformation rate with itself) and e_{ij} is the (i,j)-th component of deformation rate expressed as $e_{ij}=\frac{1}{2}\left(\frac{\partial v_i}{\partial x_j}+\frac{\partial v_j}{\partial x_i}\right)$, π_c is a critical value of π based on the non-Newtonian model, μ_β is the plastic viscosity of the fluid. This model reduces to Newtonian model for vanishing yield stress i.e. when s_y=0.

To facilitate analytical solutions, we introduce the transformation between the *laboratory frame* and *wave frame* which is given as:

$$\bar{X}-c\bar{t}\equiv\bar{x},\bar{Y}\equiv\bar{y},\bar{U}-c\equiv\bar{u},\bar{V}\equiv\bar{v},\bar{P}(\bar{X},\bar{t})=\bar{p}(\bar{x}),\ \bar{H}(\bar{X},\bar{t})\equiv\bar{h}(\bar{x}). \tag{10}$$

Furthermore we invoke the following one-dimensional physical parameters:

$$x=\frac{\bar{x}}{\lambda},\ y=\frac{\bar{y}}{a},\ u=\frac{\bar{u}}{c},\ v=\frac{\lambda\bar{v}}{ac},\ t=\frac{c\bar{t}}{\lambda},\ \ p=\frac{a^2\bar{p}}{\mu c\lambda},\ \ \beta=\frac{a}{\lambda},$$

$$h=\frac{\bar{h}}{a},\ \mathrm{Re}=\frac{\rho c a}{\mu},\ \zeta=\mu_\beta\sqrt{2\pi_c}\,/\,p_y,\ \theta=\frac{\bar{T}-\bar{T}_0}{\bar{T}_0},\ B_r=\frac{\mu\bar{u}^2}{\kappa(\bar{\mathrm{T}}-\bar{\mathrm{T}}_0)}=E_c\,\mathrm{Pr},\tag{11}$$

where $\beta,\zeta,\mathrm{Br},\mathrm{Ec},\mathrm{Pr}$ respectively denote the wave number, Casson (viscoplastic) fluid parameter, Brinkman number, Eckert number and Prandtl number. Now, employing the long wavelength and low Reynolds number assumptions, since we consider *creeping flow*, Eqs. (6-8) reduce to:

$$\left(1+\frac{1}{\zeta}\right)\frac{\partial^2 u}{\partial y^2}-(u+1)M^2\cos\Theta=\frac{\partial p}{\partial x},\tag{12}$$

$$0=\frac{\partial p}{\partial y},\tag{13}$$

$$\frac{\partial^2\theta}{\partial y^2}=-B_r\left(\frac{1}{\zeta}\frac{\partial u}{\partial y}\right)^2.\tag{14}$$

The boundary conditions are transformed to:

$$\left.\frac{\partial u}{\partial y}\right|_{y=0}=0,\quad \left.\frac{\partial\theta}{\partial y}\right|_{y=0}=0,\ u\big|_{y=h}=-1-\frac{2\pi\varepsilon\alpha\beta\cos(2\pi x)}{1-2\pi\varepsilon\alpha\beta\cos(2\pi x)}+\frac{\Lambda}{\zeta}\frac{\partial u}{\partial y},\ \text{and}\ \theta+\gamma\left.\frac{\partial\theta}{\partial y}\right|_{y=h}=0\ ,\tag{15}$$

Here the third and fourth boundary conditions are associated with the velocity slip and thermal slip conditions, respectively. The *volumetric flow rate* in the channel is defined as:

$$Q=\int_0^h u dy.\tag{16}$$

3. ANALYTICAL SOLUTIONS

Solving Eqs. (12)-(14) with boundary condition (15), exact solutions for velocity, temperature and pressure gradient can be obtained as:

$$u(x,y)=-1-\frac{dp}{dx}\frac{\sec(\Theta)}{M^2}-\left(\Omega_1\frac{dp}{dx}\left(\cosh(\Omega_2 y)-\sinh(\Omega_2 y)\right)\right)/\left(\zeta^{3/2}\left(-\cosh(\Omega_2 Mh)\right)+\Omega_3\sinh(\Omega_2 Mh)\right)-M^2\sqrt{\zeta}\cosh(\Omega_2 Mh).\tag{17}$$

$$\frac{dp}{dx}=\frac{F+A}{\Omega_7}.\tag{18}$$

$$\theta(x,y)=\frac{B_r(\zeta+1)\left(M^2S+\frac{dp}{dx}\sec(\Theta)\right)^2\left(2\zeta M^2y^2\cos(\Theta)-(\zeta+1)\cosh\left(2\sqrt{\frac{\zeta}{\zeta+1}}My\sqrt{\cos(\Theta)}\right)\right)}{\Omega_8} \quad (19)$$

$$+C_1y+C_2.$$

where:

$$S=\frac{2\pi\varepsilon\alpha\beta\cos(2\pi x)}{1-2\pi\varepsilon\alpha\beta\cos(2\pi x)},A=\frac{\Omega_9}{\Omega_{10}}.,$$

$$\Omega_1=\sqrt{\zeta}(\zeta+1)\sec(\Theta),$$

$$\Omega_2=\sqrt{\frac{\zeta}{\zeta+1}}M\sqrt{\cos(\Theta)},$$

$$\Omega_3=\sqrt{\zeta+1}\Lambda M\sqrt{\cos(\Theta)},$$

$$\Omega_4=\sqrt{\zeta}(\zeta+1)h\sec^{\frac{3}{2}}(\Theta)\cosh(\Omega_2Mh),$$

$$\Omega_5=\left(-\sqrt{\zeta+1}h\Lambda M\sec(\Theta)\sinh(\Omega_2Mh)-\frac{(\zeta+1)^{3/2}\sec^2(\Theta)\sinh(\Omega_2Mh)}{M}+\Omega_4\right),$$

$$\Omega_6=M^2\left(\sqrt{\zeta+1}\Lambda M\sinh\left(\sqrt{\frac{\zeta}{\zeta+1}}hM\sqrt{\cos(\Theta)}\right)-\sqrt{\zeta}(\zeta+1)\sqrt{\sec(\Theta)}\cosh\left(\sqrt{\frac{\zeta}{\zeta+1}}hM\sqrt{\cos(\Theta)}\right)\right),$$

$$\Omega_7=-\frac{\Omega_5}{\Omega_6},$$

$$\Omega_8=8M^4\left(\frac{\sqrt{\zeta}(\zeta+1)\cosh\left(\sqrt{\frac{\zeta}{\zeta+1}}hM\sqrt{\cos(\Theta)}\right)-\sqrt{\zeta+1}\Lambda M\sqrt{\cos(\Theta)}}{\sinh\left(\sqrt{\frac{\zeta}{\zeta+1}}hM\sqrt{\cos(\Theta)}\right)}\right)^2$$

$$\Omega_9=\frac{\sqrt{\zeta}(\zeta+1)hM\sqrt{\sec(\Theta)}\cosh\left(\sqrt{\frac{\zeta}{\zeta+1}}hM\sqrt{\cos(\Theta)}\right)-\sqrt{\zeta+1}\sec(\Theta)\sinh\left(\sqrt{\frac{\zeta}{\zeta+1}}hM\sqrt{\cos(\Theta)}\right)}{\left(h\Lambda M^2\cos(\Theta)+\zeta S+S\right)},$$

$$\Omega_{10}=M\left(\frac{\sqrt{\zeta+1}\Lambda M\sinh\left(\sqrt{\frac{\zeta}{\zeta+1}}hM\sqrt{\cos(\Theta)}\right)-\sqrt{\zeta}(\zeta+1)\sqrt{\sec(\Theta)}}{\cosh\left(\sqrt{\frac{\zeta}{\zeta+1}}hM\sqrt{\cos(\Theta)}\right)}\right)$$

$$\Omega_{11} = 2M^3 \cos^{\frac{3}{2}}(\Theta)\left(\sqrt{\zeta}(\zeta+1)\cosh\left(\sqrt{\frac{\zeta}{\zeta+1}}hM\sqrt{\cos(\Theta)}\right) - \sqrt{\zeta+1}\Lambda M\sqrt{\cos(\Theta)}\sinh\left(\sqrt{\frac{\zeta}{\zeta+1}}hM\sqrt{\cos(\Theta)}\right)\right)^2,$$

$$\Omega_{12} = \mathrm{B_r}(\zeta+1)^{3/2}\left(\frac{dp}{dx}\right)^2 \sec^{\frac{5}{2}}(\Theta)\left(\begin{array}{l}\left(\sqrt{\zeta+1}\sqrt{\sec(\Theta)} - 2\gamma\sqrt{\zeta}M\right)\left(\begin{array}{l}\cosh\left(2\sqrt{\frac{\zeta}{\zeta+1}}hM\sqrt{\cos(\Theta)}\right)\\ -\sinh\left(2\sqrt{\frac{\zeta}{\zeta+1}}hM\sqrt{\cos(\Theta)}\right)\end{array}\right)\\ +2\sqrt{\zeta}(h+\gamma)M\end{array}\right),$$

$$\Omega_{13} = 4M^4\left(\begin{array}{l}\zeta^{3/2}\sqrt{\sec(\Theta)}\cosh\left(\sqrt{\frac{\zeta}{\zeta+1}}hM\sqrt{\cos(\Theta)}\right) - \sqrt{\zeta+1}\Lambda M\sinh\left(\sqrt{\frac{\zeta}{\zeta+1}}hM\sqrt{\cos(\Theta)}\right)\\ +\sqrt{\zeta}\sqrt{\sec(\Theta)}\cosh\left(\sqrt{\frac{\zeta}{\zeta+1}}hM\sqrt{\cos(\Theta)}\right)\end{array}\right)^2,$$

$$C_1 = -\frac{\left(\frac{dp}{dx}\right)^2 \mathrm{B_r}\sqrt{\zeta}(\zeta+1)^{3/2}}{\Omega_{11}},$$

$$C_2 = \frac{\Omega_{12}}{\Omega_{13}} \tag{20}$$

The pressure rise (Δp) is computed by the following expression:

$$\Delta p = \int_0^1 \left(\frac{\partial p}{\partial x}\right) dx. \tag{21}$$

The *stream function* in the wave frame (obeying the Cauchy-Riemann equations, $u = \frac{\partial \psi}{\partial y}$ and $v = -\frac{\partial \psi}{\partial x}$) may be computed by using Eq.(17). Visualization of streamlines is achieved with Mathematica symbolic software which allows an examination of bolus formation and trapping.

4. GRAPHICAL ILLUSTRATION AND DISCUSSION

In this section we have presented distributions of pressure rise, pressure gradient, velocity,

temperature profile and streamlines for the Casson fluid parameter (ζ), Hartmann number (M), measure of the eccentricity (α), cilia length (ε), volumetric flow rate (Q), wave number (β) and Brinkman number (*Br*). Numerical integration is performed in Mathematica software for the *pressure rise per wavelength*. In the present work we do not explicitly consider the influence of magnetic field inclination (Θ) on flow characteristics. This is deferred to a subsequent study [37]. All computations are conducted with $\Theta = 2\pi$ *i.e. the magnetic field is imposed in the X-direction.*

Figs.2 (a-d) illustrate the velocity profiles under the effects of Hartmann number (*M*), velocity slip parameter (Λ), volumetric flow rate (*Q*) and measure of the eccentricity (α). Fig.2 also shows a comparative study for Casson fluids and Newtonian fluids under the same conditions. Fig. 2a indicates that the velocity increases with increasing the magnetic field in neighborhood of center line while opposite behavior is pointed out near to boundary of walls, for case of Casson fluid. With $\Theta = 2\pi$, $Cos\Theta = Cos2\pi = 1$ *and therefore the x-direction magnetic body force in eqn. (12), viz* $-(u+1)M^2Cos\Theta$ *reduces to* $-(u+1)M^2$. *This body force is retarding and orientated at right angles to the channel axis i.e. normal to the x-axis (it is perpendicular to the direction of magnetic field).* This serves to accelerate the flow in the core region and decelerate it near the boundaries, for the Casson fluid case. Velocity profile is weakly altered for Newtonian fluid and a slight deceleration is observed in the core region (around the channel centre line). Fig.2b shows the effect of velocity slip parameter (Λ) on velocity profile. Clearly velocity is enhanced in magnitude with increasing the magnitude of slip parameter in the interval $-1<y<1$ whereas the converse response is computed in the near wall zones. Therefore greater wall hydrodynamic (velocity) slip accelerates the flow in the *core region of the channel* but decelerates the flow *near the channel wall boundaries*. A similar observation has been reported by Ebaid [26] among others.

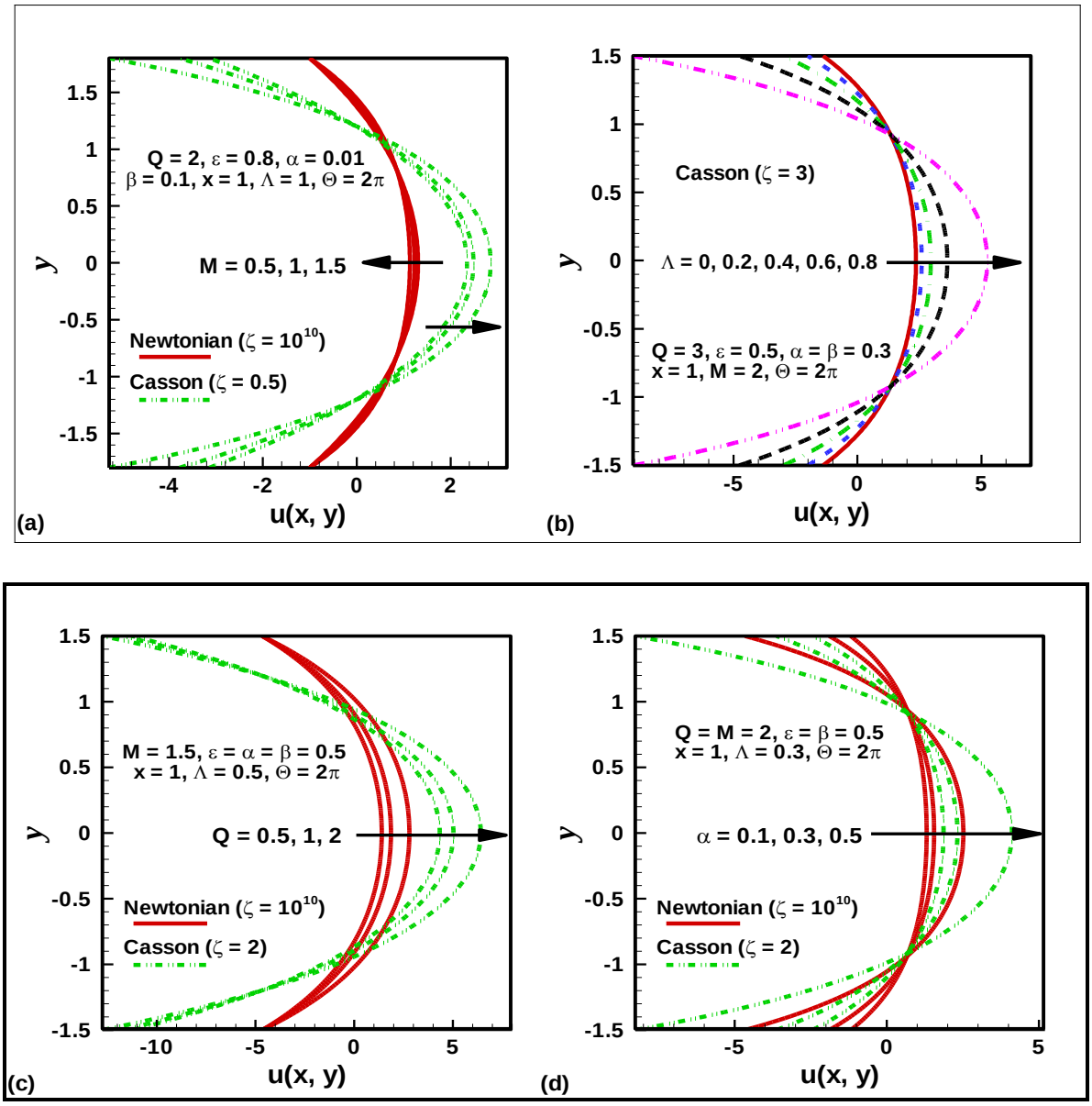

Figs.2. Velocity profile for different values of (a) Hartmann number, (b) velocity slip parameter, (c) flow rate, (d) measure of the eccentricity·

Fig.2c confirms that increasing volumetric flow rate corresponds to acceleration in the flow throughout the entire channel domain. However greater velocity magnitudes are attained at the channel wall for the Newtonian case as compared with the Casson viscoplastic fluid case. Fig.2d depicts that velocity increases with increasing the measure of the eccentricity in both cases Casson fluid as well as Newtonian fluid. It is also revealed that the velocity is greater in the core

region for Casson fluids in comparison to Newtonian fluids. Numerical solutions for velocity profile with all physical parameters are also given in **Table 1**. Here both slip and no-slip cases are documented, for a section of the upper channel half-space ($0<y<0.5$) and other parameters are also varied. With increasing cilia length (ε) velocity is observed to decrease both for the no slip ($\Lambda=0$) and slip ($\Lambda=0.5$) case; however magnitudes are significantly greater with no slip.

Table. 1. Numerical values of the velocity profile.

				$u(x,y)$	No slip $\Lambda=0$		$u(x,y)$	Slip $\Lambda=0.5$	
ε	M	α	β	$(y=0)$	$(y=0.25)$	$(y=0.5)$	$(y=0)$	$(y=0.25)$	$(y=0.5)$
0.01	2	0.5	0.3	0.34078	0.35135	0.176162	0.0308918	0.0289219	0.023012
0.05				0.30442	0.30917	0.116049	0.0284459	0.026476	0.0205662
0.1				0.24896	0.34624	0.0301369	0.0255304	0.0235605	0.0176507
	1			0.27758	0.26665	0.0317633	0.17758	0.16665	0.0217633
	3			0.30601	0.21532	0.0273027	0.20601	0.11532	0.0173027
	5			0.29880	0.13639	0.0176741	0.19880	0.03639	0.0176741
		0.1		0.29877	0.13636	0.0176717	0.00510608	0.00471209	0.00353013
		0.2		0.19877	0.13637	0.0176723	0.0102122	0.00942419	0.00706026
		0.3		0.19878	0.13637	0.0176729	0.0153182	0.0141363	0.0105904
			0	0.15493	0.12505	-0.0039357	0.06075	0.0560625	0.042213
			0.1	0.10044	0.16110	0.00434531	0.0405774	0.0374464	0.0280535
			0.2	0.14898	0.19876	0.0115899	0.0261495	0.0241318	0.0180787

With increasing eccentricity parameter (geometric cilia parameter), α, for the *no-slip* case, very little modification in velocity distribution is computed. However *with slip present*, there is a marked elevation in velocity i.e. the flow is accelerated in the upper channel half space. With increasing metachronal wave number, β, velocities are enhanced somewhat for the no slip case, whereas they generally reduced in the slip case.

Fig. 3 (a-d) present the variation of pressure rise against the flow rate under the influences of physical parameters Hartmann number, velocity slip parameter and wave number, with all other parameters invariant. Fig.3a illustrates that pressure rise is elevated with the effect of magnetic field in the case of Casson fluids whereas it is depleted for the case of Newtonian fluids in the

pumping region i.e. for $Q<0$. The opposite trends are observed in the *augmented pumping region* i.e. for $Q>0$. Pressure rise is significantly greater for Casson fluid compared with Newtonian fluid and this is probably attributable to the greater momentum required to mobilize viscoplastic fluids- however this is only the case in the *pumping region*. In the *augmented pumping region*, the opposite behavior is observed and Newtonian fluid achieves greater pressure rise than Casson fluids. Fig. 3b demonstrates that pressure rise diminishes with an increase in the velocity slip parameter (Λ), but only to a *critical value* of flow rate beyond which the reverse trend is observed, for $\Lambda>0$. However when slip is absent ($\Lambda=0$) there is a sustained decrease in pressure rise for all values of flow rate.

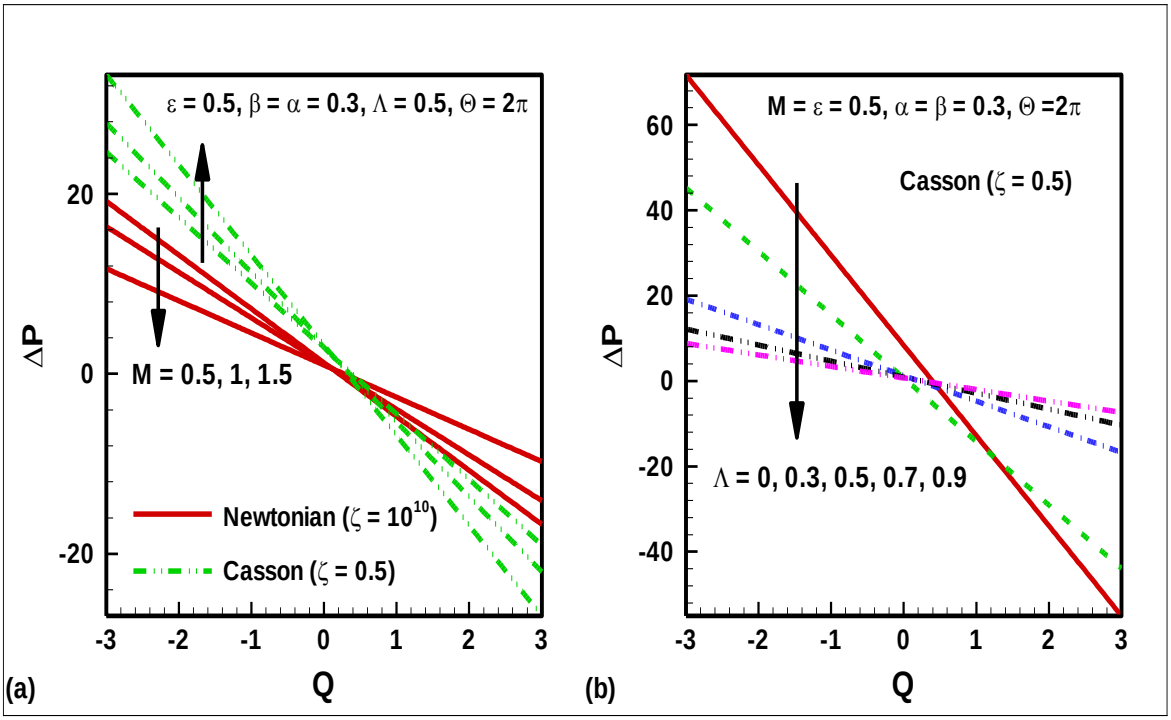

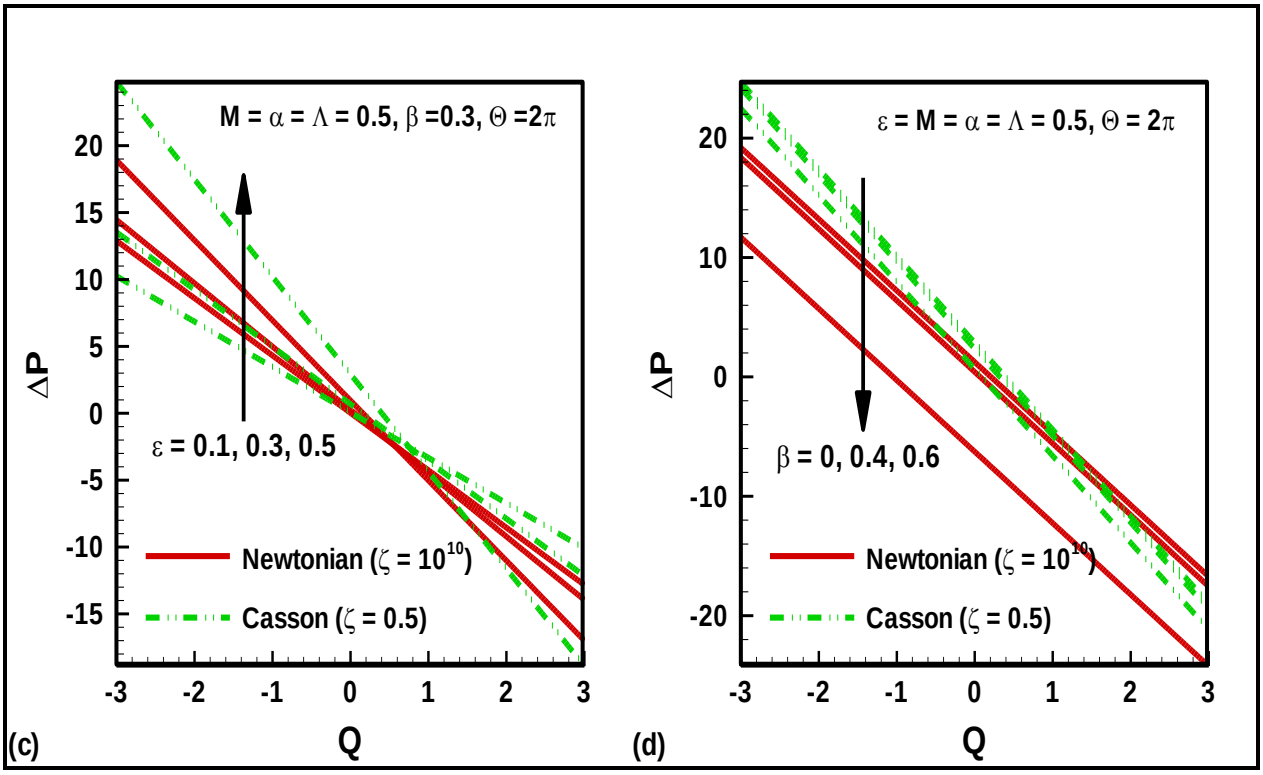

Figs.3. Pressure rise for different values of (a) Hartmann number, (b) velocity slip parameter, (c) Cilia length, (d) wave number.

Fig. 3c shows the pressure rise *increases* with increasing cilia length parameter (ε) for $Q<1$ whereas the reverse behavior is computed for $Q>1$. The Casson fluid however consistently attains the greatest pressure rise, relative to the Newtonian fluid. Fig. 3d depicts that pressure rise *reduces* with increasing the magnitude of wave number across the entire range of flowrate values (Q) and indeed this observation is consistent with many other studies on ciliary propulsion fluid dynamics [39]. The Casson fluid again achieves greater pressure rise than the Newtonian fluid.

Figs. 4(a-d) depict the distributions in pressure gradient for different values of the flow parameters. Inspection of the figures shows that magnitude of pressure gradient *increases* with an increase in Hartmann number (for the case of Newtonian fluid), flow rate, cilia length and velocity slip parameter whereas with the increase in Hartmann number (for the case of Casson

fluid), pressure gradient *decreases*. Stronger magnetic field clearly *opposes* pressure gradient build-up in Casson fluids whereas it assists it for Newtonian fluids.

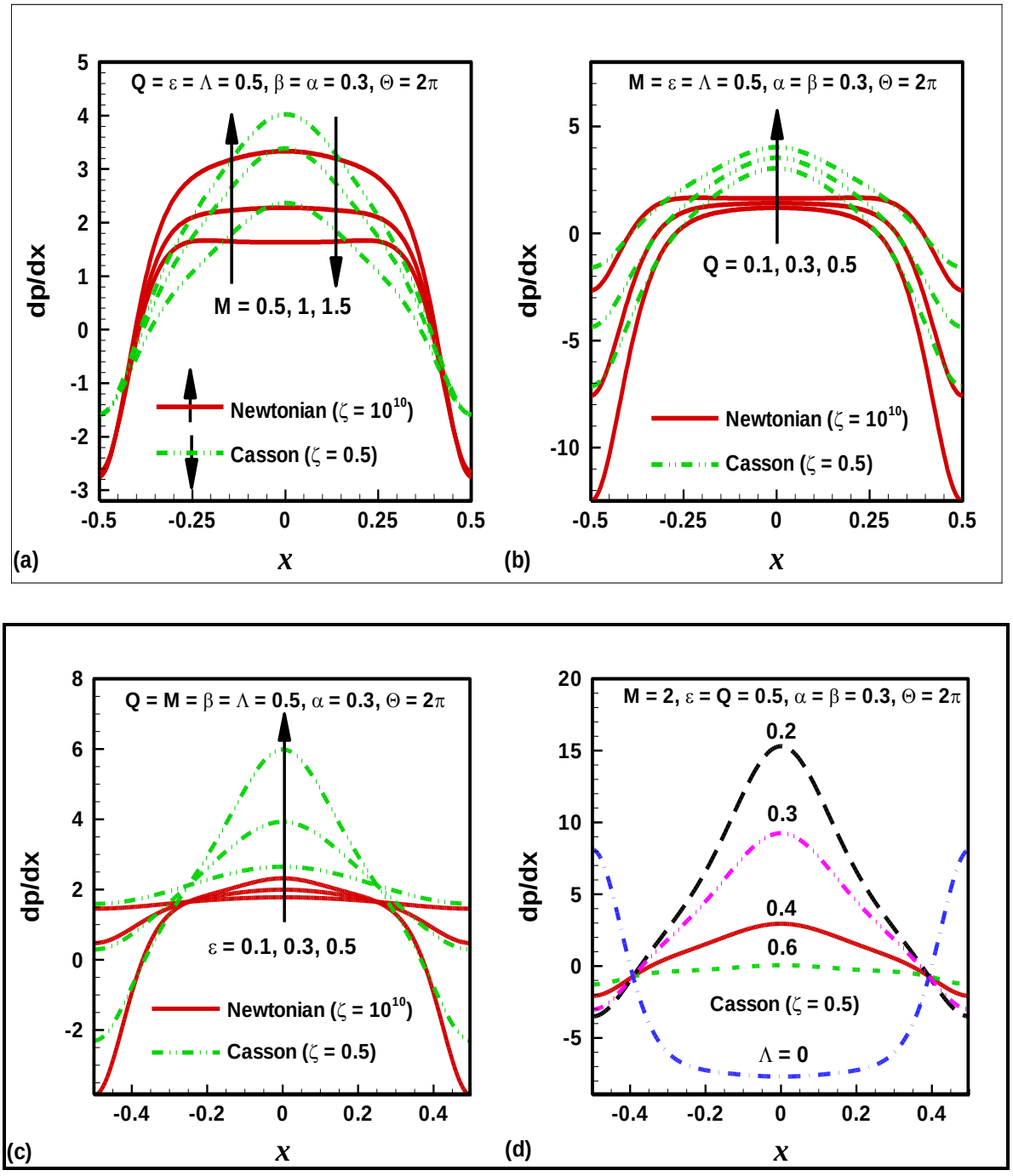

Fig.4. Pressure gradient for different values of (a) Hartmann number, (b) flow rate, (c) Cilia length, (d) velocity slip parameter.

It is also observed that the maximum pressure gradient occurs when x=0.48 and near the channel walls the pressure gradient is small. This implies that the flow can easily pass in the central region of the channel. Pressure gradient magnitudes are higher for Casson fluid compared with a Newtonian fluid. The pressure distributions for the Casson fluid are also generally more peaked whereas for the Newtonian fluid they are more oblate parabolas.

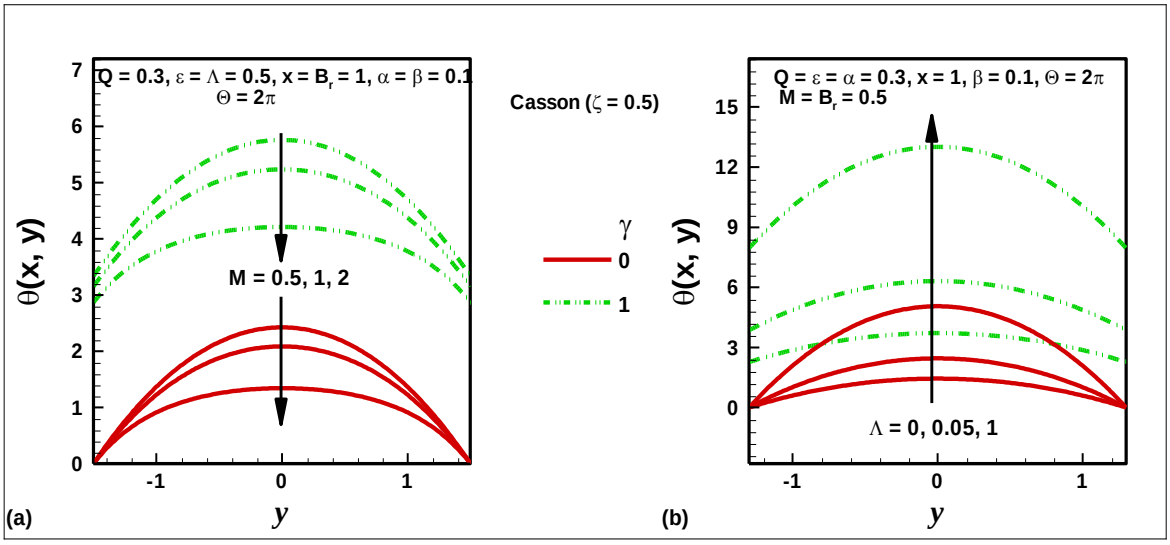

Fig.5. Temperature profile for different values of (a) Hartmann number (b) velocity slip parameter.

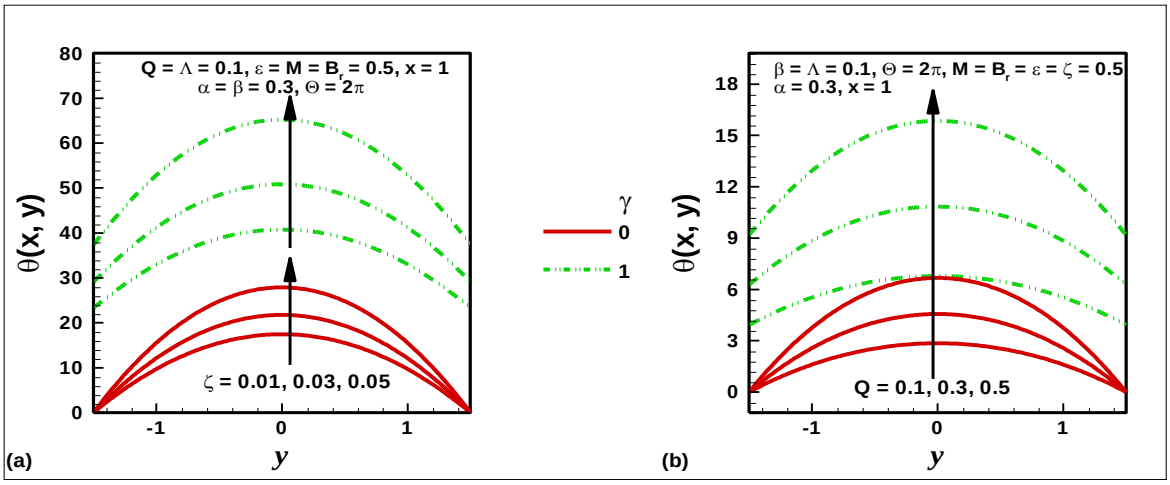

Fig.6. Temperature profile for different values of (a) Casson fluid parameter (b) flow rate.

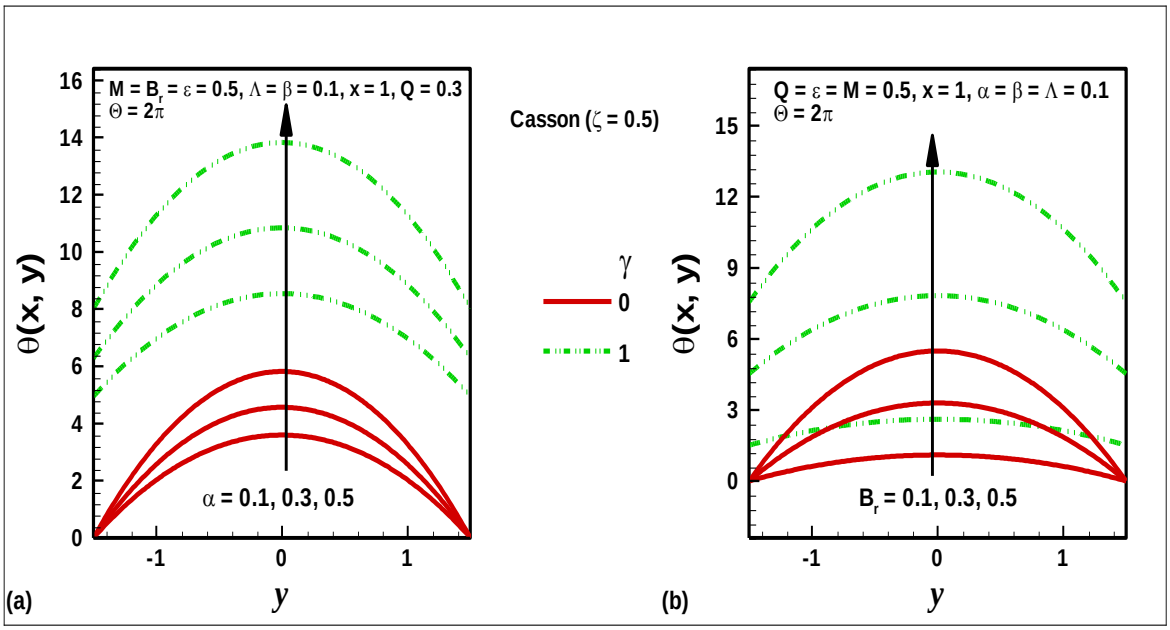

Fig.7. Temperature profile for different values of (a) measure of the eccentricity (b) Brinkmann number.

Figs 5-7 illustrate the temperature profiles for different flow parameters. The profiles are consistently parabolic across the channel span, and are similar to velocity profile which is also clear from the eq. (19). From temperature profile, a comparative study of Casson fluids and Newtonian fluids is also made. It is observed that temperature increases with the increasing the magnitude of Casson fluid parameter, flow rate, Hartmann number, velocity slip parameter, measure of the eccentricity and also Brinkman number. It is also noticed that temperature with thermal slip is of greater magnitude than for the no slip case, a pattern which has also been computed by Srinivas *et al.* [29] and Uddin *et al*. [30]. Effectively *Br* embodies the relative influence of heat produced by viscous dissipation and heat transported by molecular conduction. It therefore can be used to express the ratio of viscous heat generation to external heating in thermofluid dynamics. Higher *Br* implies a lower contribution in thermal conduction generated via viscous dissipation and greater elevation in temperatures, a trend which has been observed in many studies including Gorla *et al*. [40]. Confidence in the present computations is therefore high.

Figs. 8-10 depict the trapping and bolus evolution for different values of Hartmann number, Casson fluid parameter and slip parameter. Figs. 8(a-c) reveal that with greater Hartmann number (which corresponds to an increase in the magnetic field strength), the electromagnetic retarding force (Lorentz body force) substantially *exceeds* the viscous hydrodynamic force and this serves to inhibit bolus growth - as a result the size of the trapping bolus decreases whereas the number of boluses increases. Figs. 9(a-c) illustrate that an increase in Hartmann number (for the case of *Newtonian* fluid) increases both the size and number of trapping boluses. Figs.10(a-c) indicate that an increase in velocity slip parameter *effectively enhances* the number of boluses but decreases the size of bolus. Figs. 11(a-c) provide a visualization of the isotherms for different values of Casson fluid parameter. A line connecting points of equal temperature is called an *isotherm*. The small orange numbers are contour labels, which identify the magnitude of an isotherm (75, 85 degrees Fahrenheit). Increasing the magnitude of Casson fluid parameter i.e. *elevating* viscoplastic effect is found to *enhance* temperatures.

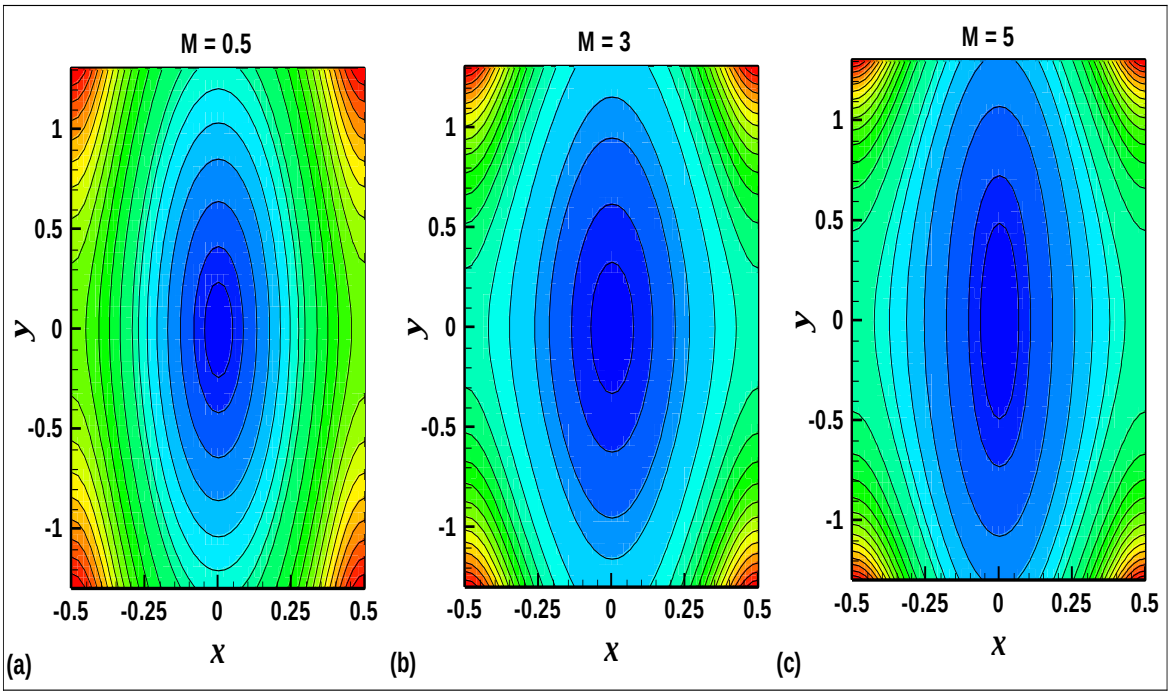

Figs.8. Streamlines for Casson fluid for different values of Hartmann number $M(0.5,3,5)$.

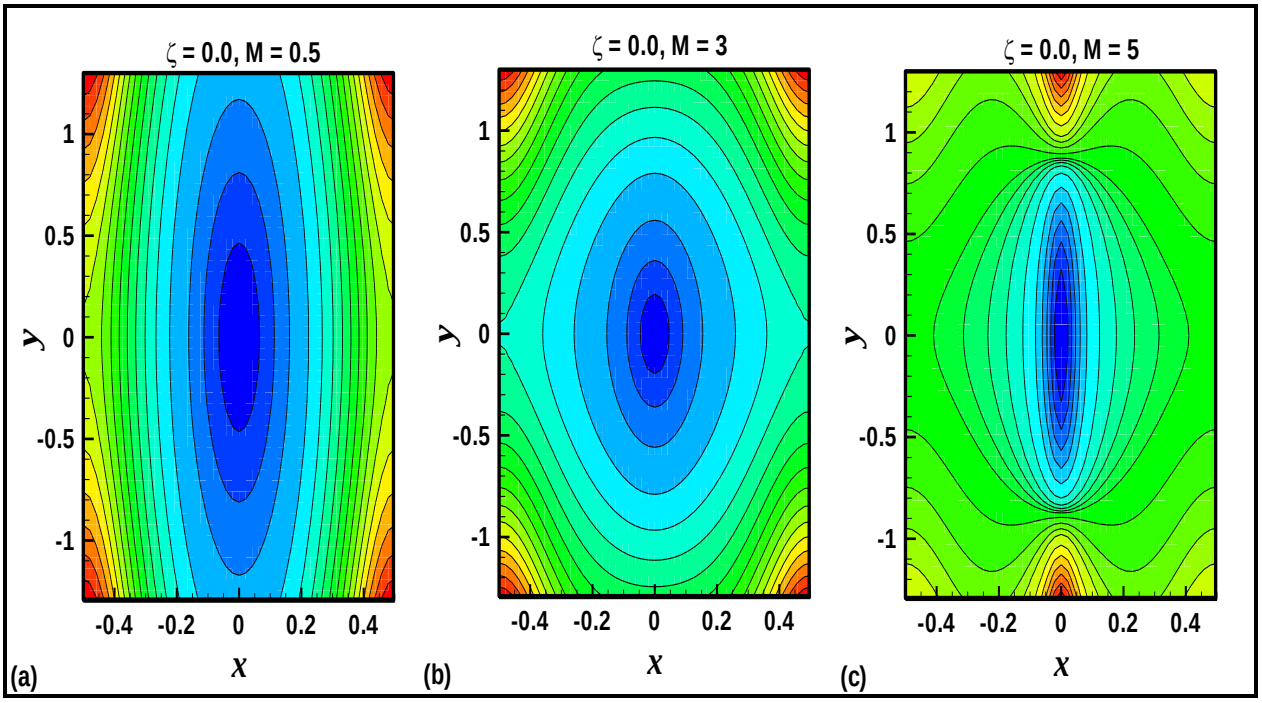

Figs. 9. Streamlines for Newtonian fluid for different values of $M(0.5,3,5)$

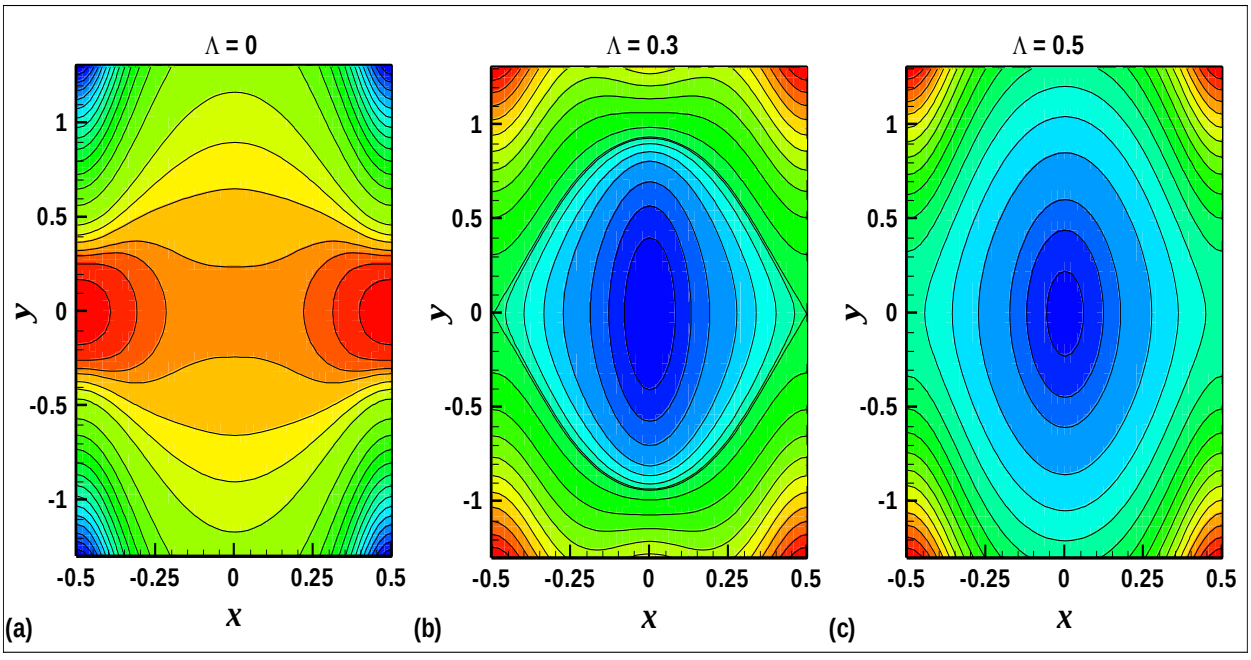

Figs.10. Streamlines for different values of velocity slip parameter $\Lambda(0,0.3,0.5)$.

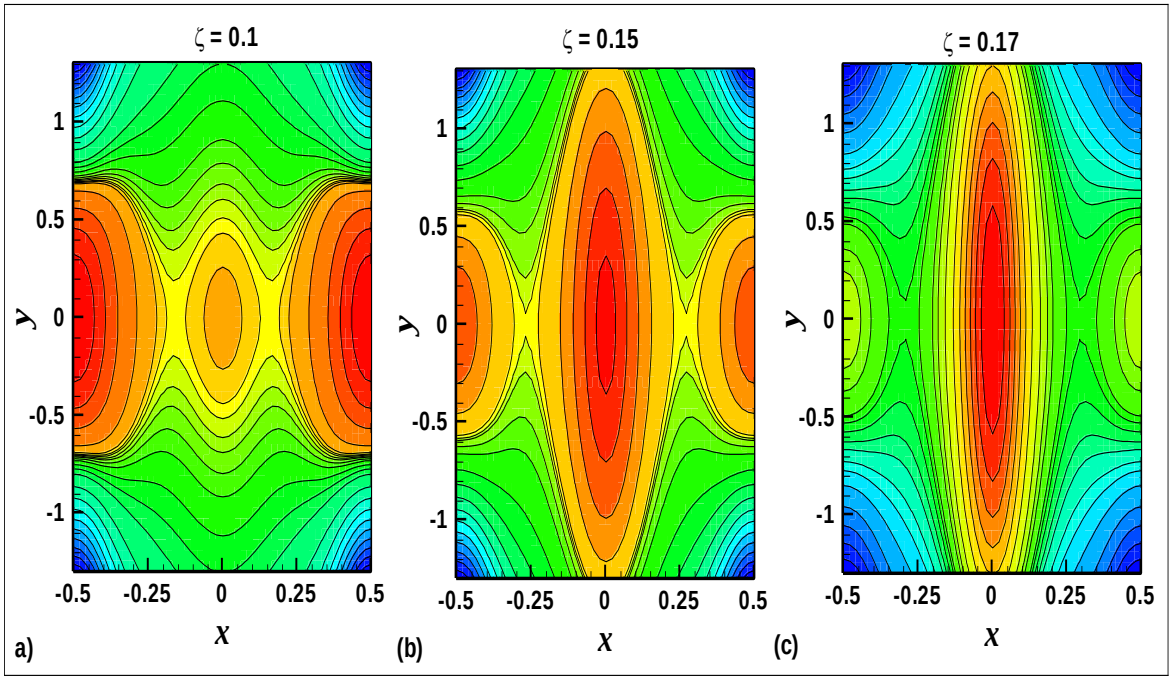

Figs.11. Isotherms for different values of Casson fluid parameter $\zeta(0.1, 0.15, 0.17)$

5. CONCLUSIONS

The magnetohydrodynamic flow and heat transfer in an electrically-conducting Casson viscoplastic fluid generated by metachronal wave propagation induced by beating cilia effect through a channel under the effect of an oblique magnetic field, has been studied theoretically. Velocity and thermal slip conditions and also viscous heating have been incorporated in the mathematical model. The linearized non-dimensional problem has been solved analytically. The computations have shown that:

1. The velocity field decreases with an increase in Hartmann number (M), velocity slip parameter (Λ), cilia eccentricity parameter (α) and volumetric flow rate (Q) in the vicinity of the channel walls whereas it increases at the center of the channel.
2. Velocity field is qualitatively similar for Newtonian and Casson fluids in view of all parameters whereas the magnitudes computed are significantly different.
3. Velocity magnitudes for Newtonian fluid are distinctly lower as compared to Casson fluids.

4. In the *pumping region* (negative volumetric flow rate), the pressure rise *decreases* with the increase of Hartmann number, velocity slip parameter and wave number whereas pressure rise *increases* with the increase in cilia length.
5. Pressure rise for a Casson (viscoplastic) fluid is generally in excess of that for a Newtonian fluid.
6. Magnitude of pressure gradient *increases* with greater Hartmann (magnetic body force) number (for the case of Newtonian fluid), volumetric flow rate, cilia length and velocity slip parameter. However with an increase in Hartmann number (for the case of Casson fluid) pressure gradient *decreases*.
7. Temperatures are elevated significantly and consistently with an increase in Casson fluid parameter, flow rate, Hartmann number, velocity slip parameter, measure of the eccentricity and Brinkmann (viscous dissipation) number.
8. Temperatures achieve substantially greater values with high thermal slip compared with no thermal slip.
9. The size and number of trapping boluses increase with an increase in viscoplasticity i.e. Casson fluid parameter.

The present computations have not considered multiple orientations of the magnetic field. These will be addressed in the future. Furthermore other viscoplastic models are available in the literature [41] which can also simulate physiological and medical device working fluids and these will also be explored.

REFERENCES

[1] M. Klysik, Ciliary syndromes and treatment, *Pathology -- Research and Practice*, 204 (2008) 77--88.

[2] A. Sleigh, *The Biology of Cilia and Flagella*, MacMillian, New York (1962).

[3] C. E. Miller, An investigation of the movement of Newtonian liquids initiated and sustained by the oscillation of mechanical cilia, *Aspen Emphysema Conf.* 10 (1967) 309–321.

[4] J. R. Blake, A spherical envelope approach to ciliary propulsion, *J. Fluid Mechanics*, 47 (1971) 199-208.

[5] J. R. Blake, Flow in tubules due to ciliary activity, *Bull Math Biol*. 35 (1973) 513-523.

[6] S. N. Khaderi, C. B. Craus, J. Hussong, N. Schorr,d J. Belardi, J. Westerweel, O. Prucker,d J. Ruhe, J. M. J. den Toondere and P. R. Onck, Magnetically-actuated artificial cilia for microfluidic propulsion, *Lab Chip*, 11 (2011) 2002.

[7] A. Dauptain, J. Favier and A. Battaro, Hydrodynamics of ciliary propulsion, *J. Fluids Struct*. 24 (2008) 1156–1165.

[8] S. N. Khaderi, J. M. J. den Toonder and P. R. Onck, Fluid flow due to collective non-reciprocal motion of symmetrically-beating artificial cilia, *Biomicrofluidics*, 6 (2012) 014106.

[9] S. N. Khaderi and P. R. Onck, Fluid--structure interaction of three dimensional magnetic artificial cilia, *J. Fluid Mechanics*, 708 (2012) 303-328.

[10] N. S. Akbar, Adil Wahid Butt, CNT suspended nanofluid analysis in a flexible tube with ciliated walls, *Eur. Phys. J. Plus,* 129 (2014) 174.

[11] N. S. Akbar, Z.H. Khan and S. Nadeem, Metachronal beating of cilia under influence of Hartmann layer and heat transfer, *Eur. Phys. J. Plus,* 129 (2014) 176.

[12] N. S. Akbar, A.W. Butt and N.F.M. Noor, Heat transfer analysis on transport of copper nanofluids due to metachronal waves of cilia, *Current NanoScience*, 10 (2014) 807-815.

[13] E.C. Bingham, *Fluidity and Plasticity*, McGraw-Hill, New York (1922).

[14] W.H. Herschel and R. Bulkley, Konsistenzmessungen von Gummi-Benzol Loesungen, *Kolloid Z*., 39 (1926) 291-300.

[15] N. Casson, *Rheology of Disperse Systems, Ed. C.C. Mill*, Pergamon Press, Oxford (1959).

[16] G.W. Scott Blair, An equation for the flow of blood plasma and serum through glass capillaries, *Nature*, 83 (1959) 613-614.

[17] R.B. Bird, G.C. Dai and B.J. Yarusso, The rheology and flow of viscoplastic materials. *Rev Chem Eng*., 1 (1983) 1-83.

[18] L.M. Srivastava and V. P. Srivastava, Peristaltic transport of blood: Casson model—II., *J. Biomechanics*, 17.11 (1984) 821-829.

[19] P. Chaturani and R. Ponnalagar Samy, Pulsatile flow of Casson's fluid through stenosed arteries with applications to blood flow, *Biorheology*, 23.5 (1985) 499-511.

[20] A.V. Mernone, J. N. Mazumdar and S. K. Lucas, A mathematical study of peristaltic transport of a Casson fluid, *Math. Comp. Modelling*, 35.7 (2002) 895-912.

[21] J.C. Misra and S. K. Pandey, Peristaltic transport of blood in small vessels: study of a

mathematical model, *Comp. Math. Applicns*., 43.8 (2002) 1183-1193.

[22] S.K. Pandey and D. Tripathi, Peristaltic transport of a Casson fluid in a finite channel: application to flows of concentrated fluids in oesophagus, *Int. J. Biomathematics*, 3.04 (2010) 453-472.

[23] C. Cottin-Bizonne *et al.,* Boundary slip on smooth hydrophobic surfaces: Intrinsic effects and possible artifacts, *Physical Rev. Lett.,* 94.5 (2005): 056102.

[24] G.D. Ngoma and F. Erchiqui, Heat flux and slip effects on liquid flow in a microchannel, *Int. J. Thermal Sciences*, 46.11 (2007) 1076-1083.

[25] J.C. Misra and G. C. Schit, Role of slip velocity in blood flow through stenosed arteries: a non-Newtonian model, *J. Mechanics in Medicine and Biology,* 7.03 (2007) 337-353.

[26] A. Ebaid, Effects of magnetic field and wall slip conditions on the peristaltic transport of a Newtonian fluid in an asymmetric channel, *Physics Letters A*, 372 (2008) 4493-4499.

[27] F. Yilmaz and M. Y. Gundogdu, A critical review on blood flow in large arteries; relevance to blood rheology, viscosity models, and physiologic conditions, *Korea-Australia Rheology J.*, 20.4 (2008) 197-211.

[28] R. Ellahi, Effects of the slip boundary condition on non-Newtonian flows in a channel, *Comm. Nonlinear Science and Numerical Simulation* 14.4 (2009) 1377-1384.

[29] S.R. Srinivas, R. Gayathri and M. Kothandapani, The influence of slip conditions, wall properties and heat transfer on MHD peristaltic transport, *Computer Physics Comm.,* 180.11 (2009) 2115-2122.

[30] M. J. Uddin, O. Anwar Bég and M.N. Kabir, Computational investigation of Stefan blowing and multiple slip effects on buoyancy-driven bioconvection nanofluid flow with micro-organisms, *Int. J. Heat Mass Transfer*, 95 (2016) 116-130.

[31] D. Tripathi, Peristaltic hemodynamic flow of couple-stress fluids through a porous medium with slip effect, *Transport in Porous Media*, 92.3 (2012) 559-572.

[32] N.S. Akbar and S. Nadeem, Thermal and velocity slip effects on the peristaltic flow of a six constant Jeffrey's fluid model, *Int. J. Heat and Mass Transfer*, 55.15 (2012): 3964-3970.

[33] N. Amalina Latiff, M. J. Uddin, O. Anwar Bég and A. I. M. Ismail, Unsteady forced bioconvection slip flow of a micropolar nanofluid from a stretching/ shrinking sheet, *Proc. IMECHE-Part N: J. Nanoengineering and Nanosystems* (2016). 11 pages. DOI:

10.1177/1740349915613817.

[34] D. Tripathi, O. Anwar Bég and J. Curiel-Sosa, Homotopy semi-numerical simulation of peristaltic flow of generalized Oldroyd-B fluids with slip effects, *Computer Methods in Biomechanics Biomedical Engineering,* 17(4) 433-442 (2014).

[35] C.Y. Lin, C.Y. Chen, Y.T. Hu and C.Y. Chen, Fluid dynamics analysis of magnetically actuated ciliated nano/micro structures for flow mixing and propulsion applications, *8th IEEE Int. Conf. Nano/Micro Engineered and Molecular Systems (NEMS), pp 590-593, Suzhou, China, April* (2013).

[36] O. Anwar Bég, Lik Sim, J. Zueco and R. Bhargava, Numerical study of magnetohydrodynamic viscous plasma flow in rotating porous media with Hall currents and inclined magnetic field influence, *Commun. Nonlinear Science and Numerical Simulation,* 15 (2010) 345-359.

[37] S.K. Ghosh, O. Anwar Bég, J. Zueco and Prasad, V. R., Transient hydromagnetic flow in a rotating channel permeated by an inclined magnetic field with magnetic induction and Maxwell displacement current effects, *ZAMP: J. Applied Mathematics and Physics*, 61 (2010) 147-169.

[38] N.T.M. Eldabe and M.G.E. Salwa, Heat transfer of MHD non-Newtonian Casson fluid flow between two rotating cylinders. *J. Phys. Soc. Japan*, 64, p. 41 (1995).

[39]. S. N. Khaderi J. M. J. den Toonder and P. R. Onck, Microfluidic propulsion by the metachronal beating of magnetic artificial cilia: a numerical analysis, *J. Fluid Mechanics*, 688 (2011) 44- 65.

[40] R.S.R. Gorla, L. Byrd and D. Pratt, Second law analysis for microscale flow and heat transfer, *Applied Thermal Engineering*, 27 (2007) 1414-1423.

[41] D. Tripathi and O. Anwar Bég, Mathematical modeling of peristaltic propulsion of viscoplastic fluids, *Proc. IMECHE- Part H; J. Engineering in Medicine,* 228 (2014) 67-88.